Observational relationships between ammonia, carbon dioxide and water vapor under a wide range of meteorological and turbulent conditions: RITA-2021 campaign

Ruben B. Schulte[1], **Jordi Vilà-Guerau de Arellano**[1], **Susanna Rutledge-Jonker**[2], **Shelley van der Graaf**[2], **Jun Zhang**[3], **and Margreet C. van Zanten**[1,2]

[1]Meteorology and Air Quality group, Wageningen University & Research, P.O. Box 47, 6700, AA Wageningen, the Netherlands
[2]National Institute for Public Health and the Environment (RIVM), Antonie van Leeuwenhoeklaan 9, 3721, MA Bilthoven, the Netherlands
[3]TNO, Postbus 15, 1755 ZG, Petten, the Netherlands

Correspondence: Margreet van Zanten (margreet.van.zanten@rivm.nl)

Abstract. We present a comprehensive observational approach, aiming to establish relations between the surface-atmosphere exchange of ammonia (NH_3) and the CO_2 uptake and transpiration by vegetation. In doing so, we study relationships useful for the ~~the~~ improvement and development of NH_3 flux representations ~~and their dependences~~in models. The NH_3 concentration and flux are measured using a novel open-path miniDOAS measurement setup, taken during the five week RITA-2021 campaign (25 August until 12 October 2021) at the Ruisdael Observatory at Cabauw, the Netherlands. After filtering for unobstructed flow, sufficient turbulent mixing and CO_2 uptake, we find the diurnal variability of the NH_3 flux to be characterized by daytime emissions (0.05 μg m^{-2}s^{-1} on average) and deposition at sunrise and sunset (-0.05 μg m^{-2}s^{-1} on average). We first compare the NH_3 flux to the observed gross primary production (GPP), representing CO_2 uptake, and latent heat flux (L_vE), representing ~~to evapotranspiration~~net evaporation. Next we study the observations following the main drivers of the dynamic vegetation response, which are photosynthetically active radiation (PAR), temperature (T) and the water vapor pressure deficit (VPD). Our findings show indication of the dominance of stomatal emission of NH_3, with high correlation between the observed emissions and both ~~net~~ L_vE (0.70) and PAR (0.72), as well as close similarities in the diurnal variability of the NH_3 flux and GPP. However, the efforts to establish relationships are hampered due to the amount of diversity of NH_3 sources of the active agricultural region and low data availability after filtering. Our findings show the need to collocate meteorological, carbon and nitrogen studies to advance on our understanding of NH3 ~~deposition~~ surface exchange and its representation.

1 Introduction

While nitrogen is an essential nutrient for the growth of plants, acting as a fertilizer, excess nitrogen deposition causes environmental damage and leads to an increased public health risk through the formation of particulate matter (Bobbink et al., 2003; Behera et al., 2013; Erisman and Schaap, 2004; Erisman et al., 2013; Smit and Heederik, 2017). When nitrogen critical loads are exceeded, excess nitrogen deposition threatens biodiversity through acidification and eutrophication of soils. When mitigation of the harmful effects of nitrogen fails, there can be serious political, economic and societal consequences, as demonstrated by the current Dutch nitrogen crisis (Stokstad, 2019). Atmospheric ammonia (NH_3) plays a key role in the deposition of nitrogen, mainly originating from agricultural activity. This is especially true in the Netherlands where NH_3 deposition accounts for about three-quarters of all nitrogen deposition (Wichink Kruit and van Pul, 2018; RIVM et al., 2019).

Efforts to mitigate the harmful effects of nitrogen deposition heavily rely on models representing the concentration and deposition of nitrogen compounds, supported by a network of concentration and surface-atmosphere exchange measurements. The surface-atmosphere exchange in such models is represented by parameterizations, which are developed, validated and improved based on advanced high-resolution observations. In the case of atmospheric ammonia, taking accurate high-resolution
5 measurements is notoriously difficult, due to the reactive nature of gaseous NH_3 causing the gas to "stick" to inlet walls of conventional instruments (Parrish and Fehsenfeld, 2000; von Bobrutzki et al., 2010). These challenges are amplified when measuring the NH_3 surface-atmosphere exchange flux (deposition or emission), where high precision is particularly important (Nemitz et al., 2004; Whitehead et al., 2008).

Recent developments in advanced instrumental techniques resolve these inlet issues by using optical open-path analyzers.
10 Swart et al. (2023) presents an intercomparison of two novel open-path measurement setups, aimed at measuring the NH_3 flux at half-hourly resolution: the RIVM-miniDOAS 2.2D and the commercial Healthy Photon HT8700E. The two setups showed very similar results, despite being widely different in their measurement principle and approach to derive the flux from concentrations, as the Healthy Photon uses the eddy covariance technique while the miniDOAS applies the flux-gradient method to line average concentration measurements over a 22 m open-path at two heights. In this study, we continue the analysis
15 of the observations of the miniDOAS system presented by (Swart et al., 2023), as the system provides reliable measurements of both the concentration and flux with a high operational uptime.

In a previous study, based on measurements from the predecessor of the miniDOAS system at the Veenkampen meteorological site in the Netherlands, we identified that the mechanisms behind stomatal exchange of NH_3 are not yet fully understood (Schulte et al., 2021). Here, we continue to study this stomatal exchange pathway by linking the observed NH_3 flux (F_{NH_3}) to
20 photosynthesis, i.e. the stomatal exchange of CO_2 and water vapor (plant transpiration). The similarities between the stomatal exchange of NH_3 and CO_2 have long been recognized (San José et al., 1991; Schrader et al., 2020). However, there are very few parallel measurements of NH_3 and CO_2 fluxes, and research into the two gases is generally conducted by separate scientific communities (Milford et al., 2001). Milford et al. (2001) performed one of the few attempts to develop a simple parameterization for both the CO_2 and NH_3 flux, but was unsuccessful to find such relations for NH_3 as the observed NH_3 flux over Scottish
25 Heathland was dominated by non-stomatal exchange. Further, Zöll et al. (2019) performed an analysis to study whether the biosphere-atmosphere exchange of total reactive nitrogen was driven by the same variables as carbon dioxide.

Our aim is to relate NH_3 and CO_2 fluxes to advance in our understanding of NH_3 stomatal exchange. These surface ~~exchange~~ exchanges require to be related to the sensible and latent heat fluxes, and the diurnal boundary layer dynamics (Vilà-Guerau de Arellano et al., 2023). Utilizing the recent developments in NH_3 measurement techniques, we combine the high-quality
30 miniDOAS F_{NH_3} observations with measurements of both CO_2 and water vapor fluxes, as well as other meteorological variables. As our data set is limited due to the diversity of weather conditions and the complexity associated to nearby multiple sources of ammonia, our analysis acts as a proof of concept. Serving as an example for the need of combined high quality NH_3 flux measurements with auxiliary measurements of CO_2, water vapor fluxes and other meteorological variables. As such we decided to guide our analysis solely using observations and keep the use of representation of processes to interpret our data to
35 a minimum. We first describe the observations, after which we link the observed F_{NH_3} to stomatal exchange, with the intention to establish relationships between the stomatal exchange of ammonia and the processes of CO_2 uptake and transpiration by vegetation. As these processes of photosynthesis are well understood, we explore how this understanding can lead to further improving the parameterization of the NH_3 stomatal exchange.

2   Characterizing the RITA-2021 campaign observations

40 ### 2.1   Site description and measurement strategy

In September 2021, the Ruisdael Land-Atmosphere Interactions Intensive Trace-gas and Aerosol measurement campaign, known as RITA-2021, took place at the Cabauw Observatory (https://ruisdael-observatory.nl/cabauw/). The Cabauw Observatory, one of the 6 sites within the Ruisdael Observatory, is located on flat grassland in the Netherlands (51.971^oN, 4.927^oE), with an average grass height of 0.1 m. The site provides a unique set of surface and upper air observations, matched by only
45 a very few station world-wide. This includes measurements of thermodynamic variables along the 213 m mast, radiation, surface fluxes, clouds and trace gasses. Surface elevation changes are at most a few meters over 20 km and the nearby region is agricultural. An overview of the Cabauw site, the instruments stationed at the site and its 50-years of observations is given in Bosveld et al. (2020).

During the campaign, 48 days of ammonia measurements are taken using the miniDOAS (Differential Optical Absorption
50 Spectroscopy) flux measurement setup (Berkhout et al., 2017), starting on 25 August until 12 October. The measurement setup and more details on the measurement campaign are described in Swart et al. (2023). In short, the miniDOAS is an
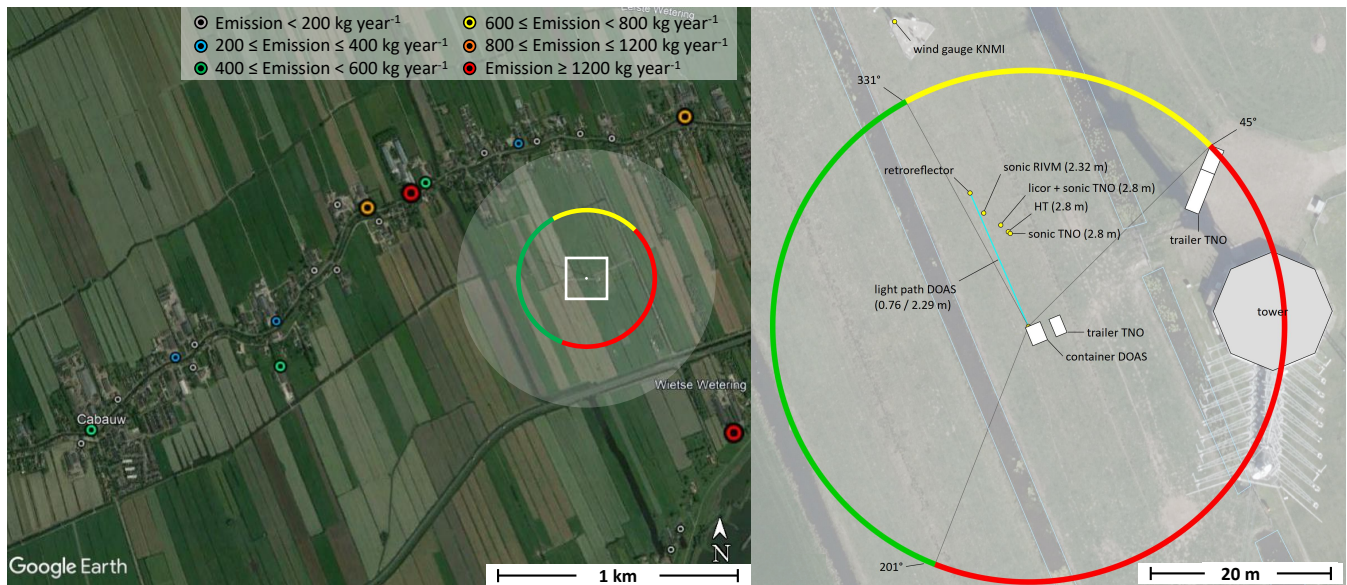
Figure 1. The area surrounding the Cabauw Observatory (left) and the setup of the instruments at the measurement site (right). The transparent white circle represents a distance of 500 m from the NH₃ measurements and the color coded dots represent the locations of nearby farms ~~, i.e.~~ whereby the emission ~~sources of~~ strength is specified in kg NH₃ per year (Source: Emissieregistratie, www.emissieregistratie.nl, last access 21 January 2022). The colored circle in both panels indicates the wind directions where the airflow towards the miniDOAS light-path is obstructed by either other instruments (yellow) or larger structures such as the tower and containers (red). (Source left panel: "Cabauw Observatory", 51.971°N, 4.927°E. © Google Earth, 27 January 2022, Image by Landsat / Copernicus. Source right panel: Swart et al. (2023), modified)

optical instrument, measuring the line average concentration (mass density) over a 22 m open path from instrument to its retroreflector. The 30 minute average NH₃ concentrations have an accuracy of ~~0.01~~ 3% (e.g. 0.15 μg m⁻³ at the median NH₃ concentration of 5 μg m⁻³ during the campaign, for further details see Swart et al. (2023). The flux measurement setup uses two miniDOAS instruments, which measure the concentration over parallel paths at different heights, i.e. 0.76 m and 2.29 m respectively. Regular intercalibrations between the miniDOAS instruments allowed quantification of and correction for any potential bias between the two instruments. The remaining random uncertainty in the Δ NH3 was 0.088 μg m⁻³ (1σ; for further details see Swart et al. (2023). F_{NH_3} is then inferred using the flux-gradient method, based on the Monin–Obukhov similarity theory (Moene and Van Dam, 2014). The flux-gradient method combines the observed vertical NH₃ gradient with turbulent measurements of a sonic anemometer (model Gill WindMasterPro™ Gill Instruments, Lymington, UK) (Wyers et al., 1993; Nemitz et al., 2004; Wichink Kruit et al., 2007; Schulte et al., 2021). The sonic anemometer was mounted at 2.8 m above the ground alongside the mini-DOAS measurement path. Temperature data is based on the corrected air temperature as calculated by the EddyPro software from the sonic data. The 10 Hz open-path H₂O and CO₂ analyser (LI-7500DS, LI-COR Biosciences,Lincoln, USA) was placed at a similar height, 15 cm away from the sonic (for more details see information over sonic #1 in (Swart et al., 2023)) The CO₂ and water vapor fluxes and other micrometeorological parameters were calculated using EddyPro software (LI-COR Bio-sciences) at 30-min intervals using the 10 Hz raw data. The ~~general~~ flux calculation procedure followed the ~~standard FluxNet methodology (McDermitt et al., 2011).~~ general best practices as applied across the FluxNet network (e.g. Mauder et al. (2022)) including co-ordinate rotation (Wilczak et al., 2001), spectral corrections for both filtering (Moncrieff et al., 2004) and low pass filtering (Moncrieff et al., 1997) and addition of the Webb–Pearman–Leuning density term (Webb et al., 1980).

The measurement field and its surroundings are shown in Fig. 1. The miniDOAS light paths are aimed in north-northwestern direction (right panel) to ensure unobstructed flow for wind coming from the west, which is the dominant wind direction in the Netherlands. North of the light path, shown in yellow in Fig 1, the flow of air is obstructed by several instruments, including the aforementioned sonic anemometer. To the east and south, the airflow is obstructed by a trailer, the 213 m high meteorological tower and the container which houses the miniDOAS instruments. The unobstructed region west of the measurement field, is mainly characterized by actively managed agricultural grassland and the small town of Cabauw (about 750 inhabitants), as shown left in Fig. 1. Several farms can be seen northwest and west of the measurement field, with varying emission strengths

Table 1. Filter criteria, being applied in sequence; with ~~the~~ filter acceptance rates (in percentages and hours).

#	Filter	Criterion	Acceptance	
			[%]	**[hours]**
-	Unfiltered observations	-	100 %	1152
Discard 1:	miniDOAS intercalibration	-	65 %	746
Discard 2:	Fertilization events 11 - 12 September	-	61 %	698
Filter 1:	Wind direction	$331^o \geq U_d \geq 201^o$	16 %	188
Filter 2:	Rain duration	$t_{rain} \leq 5\,min$	16 %	179.5
Filter 3:	Turbulent mixing	$u_* > 0.1\,ms^{-1}$	13 %	151
Filter 4:	Gross primary production	$GPP > 0\,mgCm^{-2}s^{-1}$	11 %	123.5
Filter 5:	Incoming short-wave radiation	$SW_{in} > 10\,Wm^{-2}$	9 %	102

up to over 1200 kg NH_3 year^{-1}. Sheep and cattle graze on these agricultural fields, which are actively maintained and fertilized. These activities were not documented and sporadic fertilization events do affect the NH_3 measurements, as will be discussed later.

2.2   Data filtering

5 We apply several filter criteria to the RITA-2021 observations, which are shown in Table 1 with acceptance rates for each individual filter criterion. The miniDOAS flux setup requires several days of intercalibration measurements, as described in Swart et al. (2023). No ammonia flux can be inferred from these intercalibration measurements, leaving 65% of the campaign observations suitable for flux measurements. We furthermore discard observations from 11 - 12 September, as these NH_3 emission fluxes are outliers with respect to the average observed NH_3 flux, indicating towards a fertilization event in close
10 proximity to the measurement site.

The remaining measurements are processed by applying 5 filters in total. The use of the flux-gradient method requires unobstructed upwind air flow with sufficient turbulent mixing. Figure 1 shows that the instruments were positioned anticipating winds from the south-west (green), with the obstacles located east (red) and north (yellow) of the miniDOAS optical path. We therefore apply a criterion filtering for wind directions between 201º and 331º. This filter leads to a large reduction of data
15 available for analysis, decreasing the available data from 61 % to 16 % as the prevalent wind direction during the campaign was from the north-east. As a secondary effect of this filter, the available observations are taken under synoptic weather conditions characterized by frontal passages with some rain events. The second filter excludes rain events lasting more than 5 min, as rain droplets can obstruct the light path of the miniDOAS. Finally, sufficient turbulent mixing is one of the main requirements for flux measurement using the flux-gradient method. The third filter therefore requires the friction velocity to have a value of at
20 least 0.1 m s^{-1} (u$_* \geq$ 0.1 m s^{-1}). With these three filters, we ensure the quality of the ammonia measurements, observing the NH_3 flux with an ~~accuracy of 0.01~~ average precision of 0.015 μg m^{-2}s^{-1} (1σ; for further details see (Swart et al., 2023)).

The fourth and fifth filter criteria focus on the ammonia surface-atmosphere exchange pathways. The NH_3 flux follows three pathways: the stomatal pathway, external leaf surface pathway and the soil pathway (Nemitz et al., 2001; Massad et al., 2010; van Zanten et al., 2010). The latter is generally assumed to be negligible for the F_{NH_3} over grass, as the dense
25 vegetation completely covers the soil. The external leaf ~~pathways~~pathway, represents exchange of ammonia with a thin film of water and leaf surface waxes on the leaf surface, ~~depending~~ and depends on the relative humidity (RH) (Van Hove et al., 1989). Finally, the stomatal pathway represents exchange of NH_3 through the plant stomata with ammonium dissolved in the apoplast fluids of the plant (Farquhar et al., 1980; Wichink Kruit et al., 2010). ~~While these processes happen at very small scales, at micrometer or milometer level, they can be represented at~~ These processes occur at the leaf scale
30 (micrometer or millimeter level) and as such require a representation of photosynthesis and stomatal aperture that requires to be evaluated with observations (Vilà-Guerau de Arellano et al., 2020). The upscaling to the canopy level, ~~i. e. at field scale (Vilà-Guerau de Arellano et al., 2020).~~ allows it to be compared with observations inferred from eddy-covariance such as GPP (Filter 4).

The NH_3 exchange through the stomatal pathway is governed by the dynamic response of vegetation to meteorological
35 conditions and is closely related to photosynthesis. The stomata open during the day in response to solar radiation, as the vegetation uses energy for photosynthesis, particularly the photosynthetically active radiation (PAR) (Hsiao, 1973; Cowan and Farquhar, 1977; Papaioannou et al., 1996; Ronda et al., 2001). Plants ingest CO_2 through the stomata, but water from inside the plant can evaporate as the stomata are opened. The plant can reduce this loss of water by (partly) closing the stomata in case of high water vapor pressure deficit (VPD), or increase the evaporation rate by actively opening the stomata. Increasing the
40 evaporation rate provides cooling, lowering the leaf temperature to reach optimal conditions to perform photosynthesis (Jacobs

Table 2. A characterization of the meteorology of the 17 unique days at which ~~any number of observations~~ observational data passes the filters, with the 17 day average and the range of the diurnal minimum/maximum of several (meteorological) variables. ~~A requirement~~ Daily maximum flux footprint length (70%) refers to the maximum upwind distance in meters encompassing the source area that contributed 70% of ~~non-zero net radiation is set for~~ the measured flux. For GPP and flux footprint ~~anemometer, due to the measurement uncertainty of these variables during stable nights~~ length night time are excluded.

Variable	Symbol	Diurnal minimum/maximum			
		17-day average		17-day range	
Daily minimum temperature	T_{min}	11.5	^{o}C	5.6 - 16.7	^{o}C
Daily maximum temperature	T_{max}	19.7	^{o}C	13.6 - 25.5	^{o}C
Daily maximum wind speed	u	4.5	m s^{-1}	2.2 - 7.2	m s^{-1}
Daily maximum net radiation	Q_{net}	295	W m^{-2}	137 - 400	W m^{-2}
Daily maximum sensible heat flux	H	99	W m^{-2}	27 - 173	W m^{-2}
Daily maximum latent heat flux	L_vE	145	W m^{-2}	83 - 230	W m^{-2}
~~Daily~~ Daytime maximum gross primary production	GPP	0.78	mgC m^{-2} s^{-1}	0.57 - 1.4	mgC m^{-2} s^{-1}
Daily maximum water vapor pressure deficit	VPD	966	Pa	365 - 1420	Pa
Daytime maximum ~~sonic anemometer footprint~~ flux footprint length (70 %)	$fp_{70\%}$	148	m	88 - 255	m

and de Bruin, 1997; Takagi et al., 1998; de Groot et al., 2019; Vilà-Guerau de Arellano et al., 2020). As the temperature and VPD are often highest in the ~~late~~ afternoon, the stomata often partly close to manage the loss of water. During the night, there is no PAR for photosynthesis, so the stomata are closed. As a result, the characteristics of ammonia surface-atmosphere exchange ~~of NH₃~~ differ between day and night, with the stomatal pathway being dominant during the day and the external leaf pathway being the dominant pathway during the night and in the early morning.

The uptake of CO₂ is represented by the Gross Primary Production (GPP), in mgC m^{-2}s^{-1}. The GPP and the ~~(soil) CO₂ respiration (RESP~~ ecosystem respiration (ER) combined define the Net Ecosystem Exchange (NEE) of CO₂~~, following $NEE = GPP + RESP$, which is measured as~~ the CO₂ flux. ~~The CO₂~~. Using the sign convention that the flux towards the surface is positive, we define the net ecosystem exchanges as: $NEE = GPP + ER$ where under normal daytime grassfield conditions our observations are NEE > 0, and the inferred GPP are positive and ER negative, respectively. The ecosystem respiration is estimated by taking the average campaign nighttime (defined when the net available radiation is zero, $Q_{net} < 0$) CO₂ flux, which is approximately ~~2.2 mgCO₂~~ - 0.6 mgC m^{-2} s^{-1}. The GPP is then estimated by ~~subtracting this respiration estimate from~~ combining the observed CO₂ flux ~~, or $GPP = NEE - RESP$. Note that a positive GPP (carbon uptake) corresponds to a observed negative~~ with the estimated respiration.

The approach described above, fits with our aim to guide the analysis by measurements only. However, well-established methods exist to partition NEE into GPP and ER. In appendix A we show that using the Arrhenius-type relationship between temperature and nighttime CO₂ flux ~~(CO₂ deposition).~~ to describe ER as proposed by Lloyd and Taylor (1994), and then subtracting that from NEE to arrive at GPP, only changes the GPP estimates slightly. Because of its limited impact on the results, we continue with the observation-based estimate of GPP in the main text.

To capture observations with active stomatal exchange, Filter 4 is set to only accept GPP > 0 mgCO₂ m^{-2} s^{-1}. Due to the uncertainty of our GPP estimate, there are still some night-time observations which pass the filter. We therefore add an additional 5th filter using incoming shortwave radiation (SW_{in}). Only measurements with $SW_{in} > 10$ W m^{-2} will pass, in order to filter out these last remaining night-time observations.

After filtering, 102 hours (9 %) of all RITA-2021 observations, or 18 % of all daytime RITA-2021 observations, are available for analysis. These observations are taken over 17 unique days, spanning 29 August to 30 September, with an average of 6 hours and a maximum of 12 hours of accepted measurement per day.

2.3 Characterization of the campaign meteorology

The summer months (June, July and August) leading up to the RITA-2021 campaign are characterized as an average Dutch summer, with average temperatures (17.7 ^{o}C), above average precipitation (244 mm accumulated) and below average hours of sunshine (618 hours). Additionally the ground and surface water levels are actively managed in order to sustain optimal conditions for the agricultural activity in the area (Brauer et al., 2014). It is therefore expected that the role of long-term vegetation stress on stomatal exchange is negligible during the RITA-2021 campaign.

As discussed in Section 2.2, high temperatures or VPD can induce vegetation stress during the campaign. We therefore characterize the meteorological conditions of the 17 unique days in which the 102 hours of filtered measurements were taken. The meteorological conditions of these days are summarized in Table 2, which shows the 17 day average and the observed

range of the diurnal minimum/maximum of several variables. The 17-day average values provide a characterization of mild meteorological conditions with no indication that the vegetation is under stress. Additionally, Table 2 includes an estimate of the maximum daytime footprint of determined using the sonic anemometer , fluxes at a height of 2.8 m, following the method from Kljun et al. (2015). This footprint refers to the maximum upwind distance in meters encompassing the source area that

5 contributed 70% of the measured flux and serves as a first-order approximation of the footprint of the NH$_3$ flux measurements. The footprint shown in Table 2 is the 70 % footprint of the sonic anemometer at a height of 2.8 m, following the method from Kljun et al. (2015).

As the filtered campaign measurements are characterized by frontal passages, the weather conditions range from clear sky summer conditions with moderately high temperatures, to colder cloudy days with short precipitation events (not shown).

10 Furthermore, the atmospheric stability for the 102 hours of filtered measurements is classified using the measured Obukhov length (L) and the height of the sonic anemometer (z = 2.8 m). In total, 4.5 hours (4 %) can be classified as stable (z/L > 0.05), 61 hours (60 %) as neutral (-0.05 ≤ z/L ≤ 0.05) and 36.5 hours (36 %) as unstable conditions (z/L < -0.05). This variation leads to a large spread in all variables shown in Table 2, as indicated by the column showing the 17-day range.

2.4 ~~Characterization~~ General characterization of the NH$_3$ observations

15 The variety in meteorological conditions could be an explanation of the large day-to-day difference in the observed NH$_3$ concentrations, shown in Fig. 2b. The histogram is highly skewed and shows that most observed NH$_3$ concentrations are below 7 μg m^{-3}, ~~with a long tail leading to a maximum concentration~~ however higher concentrations with a maximum value of 24.7 μg m^{-3} are also present. Still, the mean (solid line) and median (dotted line) concentrations do indicate that the concentration decreases during the day, until the late afternoon. This would be in line with observations at several other sites, both in the

20 Netherlands (Wichink Kruit et al., 2007; Schulte et al., 2021) and in other countries, e.g. Scotland (von Bobrutzki et al., 2010) or Italy (Ferrara et al., 2021). The large day-to-day differences in the NH$_3$ measurements could be a result of the changing meteorological conditions, the nearby agricultural activity, or a combination of both.

Despite the high variability in the NH$_3$ concentration measurements, a consistent diurnal variability is observed in the NH$_3$ gradient (ΔNH$_3$) and corresponding flux in Fig. 2c and 2d. Both Fig. 2b and 2c indicate that the observed ΔNH$_3$ is independent

25 of the absolute NH$_3$ concentration, i.e. high absolute concentrations do not lead to a large concentration difference between the two miniDOAS instruments. The average diurnal variability is characterized by negative ΔNH$_3$ (deposition) in the early morning and late afternoon and positive (emission) ΔNH$_3$ during the afternoon, with a typical range of about 0.5 μg m^{-3} in both directions. In total 79 % of the filtered observations have a positive ΔNH$_3$, corresponding to NH$_3$ emissions.

As F$_{NH_3}$ is directly inferred from ΔNH$_3$, the diurnal variability in Fig. 2c and d is very similar. The NH$_3$ flux typically

30 reaches its maximum around noon at little over 0.05 μg m^{-2}s^{-1} on average, with individual noon observations ranging from -0.01 μg m^{-2}s^{-1} to 0.14 μg m^{-2}s^{-1}. Note that the measurements taken on 11 - 12 September, the aforementioned fertilization event, are approximately a factor 4 larger than the mean campaign values. Despite the large observed F$_{NH_3}$ on these days, the observed concentrations are only slightly larger than the campaign averages. These two days will not be included in the analysis presented in this study, but they are shown as an illustration of how fertilization events can impact our analysis.

35 2.5 Characterization of the ammonia flux

The main drivers of ammonia surface-atmosphere exchange are turbulent mixing, as well as the difference between the atmospheric NH$_3$ concentration and the so called canopy compensation point, i.e. an internal NH$_3$ concentration (Farquhar et al., 1980; Nemitz et al., 2001; Wichink Kruit et al., 2007). A compensation point lower than the atmospheric concentration leads to deposition of ammonia and vice-versa. The canopy compensation point consists of individual

40 compensation points for each of the individual flux pathways. Following parameterizations of the stomatal compensation point, we find it related to the (leaf) temperature and some form of nitrogen input parameter (actual or long-term NH$_3$ concentration). The stomatal compensation point increases non-linearly with increasing temperature or nitrogen input (Nemitz et al., 2001; Massad et al., 2010; van Zanten et al., 2010). As the stomatal compensation point increases and becomes larger than the atmospheric NH$_3$ concentration, or as the atmospheric concentration drops below this compensation point,

45 emission will be observed from the stomatal exchange pathway.

In Fig. 3a, we show the observed ammonia flux against the ~~observed temperatureof the sonic anemometer~~air temperature, with the colors indicating the atmospheric NH$_3$ concentration at 2.29 m. Despite our efforts to filter for observations where the stomatal pathway is dominant, it ~~is possible~~ cannot be ruled out that the external leaf pathway still plays an important role in the morning, through deposition onto morning dew at canopy level (van Zanten et al., 2010; Wentworth et al., 2016). We therefore

50 use black circles to mark observations taken before 12:00 UTC with RH > 80 % in Fig. 3. These highlighted observations indeed generally correspond with measurements of deposition or weak emission, indicating that NH$_3$ exchange through the
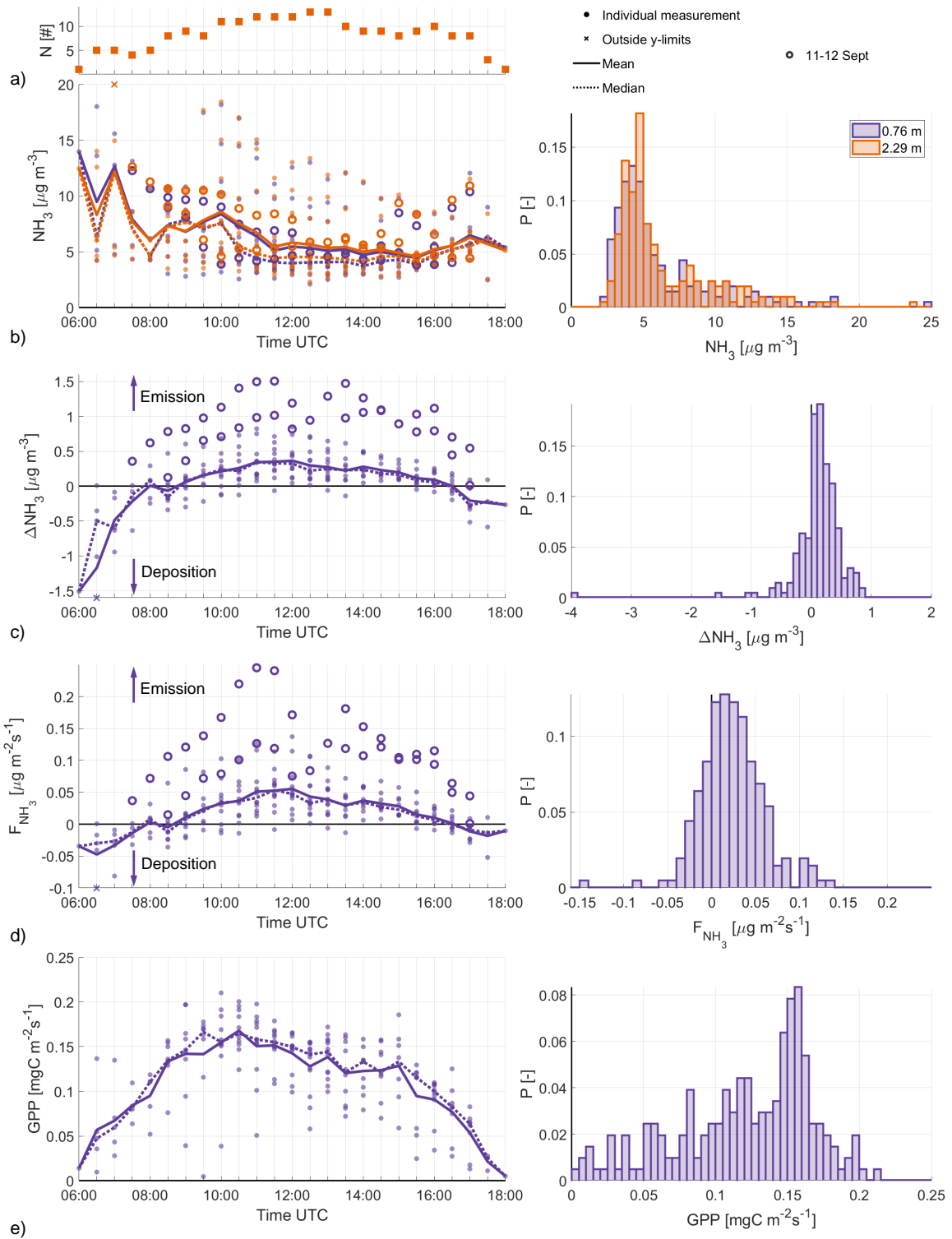
Figure 2. The diurnal variability from sunrise (6:00 UTC) to sunset (18:00 UTC) of the filtered NH_3 concentration (b), NH_3 gradient (c), F_{NH_3} (d) and the GPP with the corresponding histogram to the right. At each moment in time, the multi-day mean (solid line) and median (dotted line) are calculated. Highlighted are observations from the fertilization event at 11 - 12 September (open circles). The N number of observations over which these averages are calculated are displayed at the top (a). ΔNH_3 is defined so the sign matches that of F_{NH_3} i.e., negative numbers indicate deposition and positive numbers indicate emission.
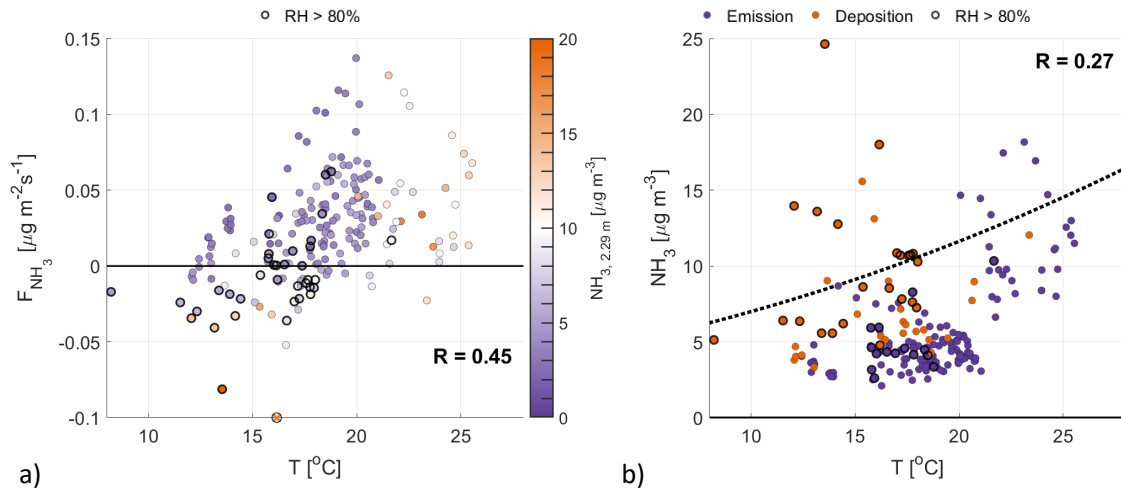
Figure 3. The 2.8 m temperature plotted against F$_{NH_3}$ (a) and observed NH$_{3, 2.29\,m}$ ~~concentration~~ (b). The color coding in (a) represents the NH$_3$ concentration, observed at 2.29 m. In (b), the dotted line represents the theoretical stomatal compensation point (χ_s) for a long-term NH$_3$ concentration of 7.7 μg m^{-3}. Highlighted with black circles are observations with RH > 80%, taken before noon, where NH$_3$ exchange through the external leaf pathway can play a significant role.

external leaf pathway is still significant for these observations. While the inclusion complicate our analysis of stomatal NH$_3$ exchange, they are still included in the analysis as it also offers an opportunity to test if the relations found in the filtered dataset differ for the marked- and unmarked observations. If that is the case, it shows we are indeed able to attribute the unmarked observations to stomatal exchange.

5   Figure 3a shows ~~that the observed F$_{NH_3}$~~ F$_{NH_3}$ to increases with temperature for low atmospheric concentration (2 μg m^{-3} ≤ NH$_{3, 2.29m}$ ≤ 7 μg m^{-3}). We attribute this increase in NH$_3$ emissions to the change in ΔNH$_3$ for increasing temperature, i.e. the difference between the approximately constant atmospheric NH$_3$ concentration and stomatal compensation point. ~~This is indeed shown in~~ Following parameterizations of this compensation point, we find it related to the (leaf) temperature and some form of nitrogen availability parameter (e.g. actual or long-term NH$_3$ concentration); increasing non-linearly with increasing

10 temperature or nitrogen input (Nemitz et al., 2001; Massad et al., 2010; van Zanten et al., 2010). In Fig. 3b ~~, where the~~ a the-oretical stomatal compensation point (dotted line) ~~increases with temperature. Here, the compensation point is calculated~~ is added. Calculated following the DEPosition of Acidifying Compounds (DEPAC) parameterization (van Zanten et al., 2010), using ~~the sonic anemometer~~ air temperature and campaign median NH$_{3, 2.29\,m}$ (7.7 μg m^{-3}).

      ~~This relation is scattered~~ F$_{NH_3}$ shows more scatter for measurements taken at high temperatures (> 21 °C). While ~~there~~

15 ~~were~~ Fig. 3b shows only small variations in the NH$_3$ concentration for temperatures below 21 °C, NH$_3$ concentration for these warmer temperatures are higher than the campaign average (> 7 μg m^{-3}) and highly variable. As the NH$_3$ flux is directly related to the difference between the atmospheric NH$_3$ and the stomatal compensation point, the variability in the atmospheric concentration lead to the scatter shown in Fig. 3a, where higher NH$_3$ ~~observations~~ concentrations correspond to weaker emission fluxes.

20 ## 3   Ammonia flux relationships to dynamic vegetation responses

The diurnal pattern of F$_{NH_3}$ in Fig. 2d shows similarities with the diurnal variability of the GPP in Fig. 2e. To further study the role of stomatal exchange during the campaign, we link the observed F$_{NH_3}$ to the dynamic vegetation responses. First, we relate the ammonia flux to the GPP, the latent heat flux (L$_v$E) and the sensible heat flux (H). The GPP and (the transpirational part of) L$_v$E are directly governed by the opening and closing of the stomata and represent stomatal exchange. Given the low

25 data availability (9%), we are aware that the analysis could be dominated by variations resulting from the diurnal variability of the fluxes. We therefore also include H in our analysis. The sensible heat flux is only indirectly related to the dynamic vegetation response through the surface energy balance, as the available energy from (solar) radiation and the soil heat flux is split between L$_v$E and H. If the observed fluxes are indeed regulated through the opening and closing of stomata, the analysis for F$_{NH_3}$ to L$_v$E and GPP should differ from the comparison with H.
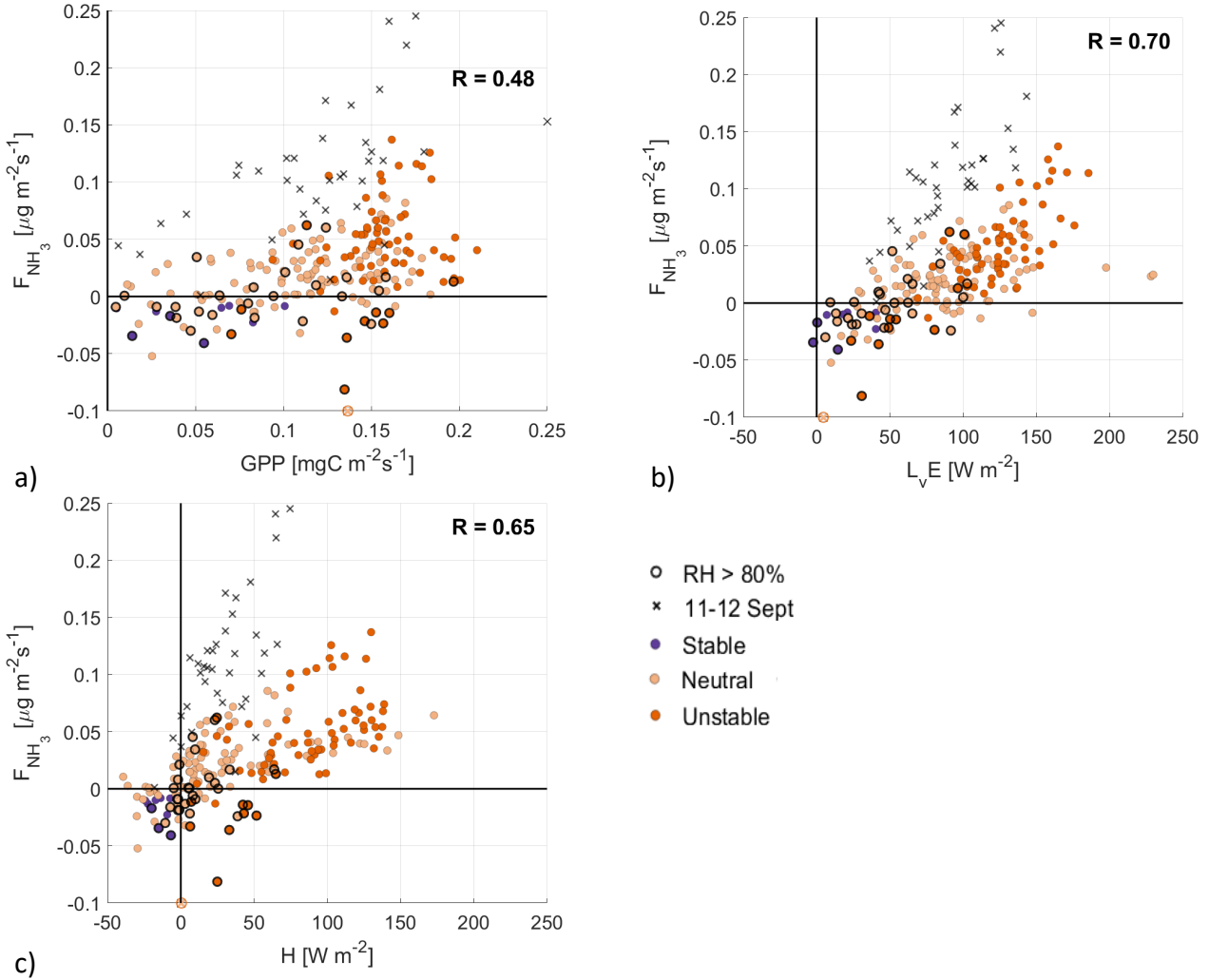
Figure 4. Scatter plots of F_{NH_3} against the GPP (a), L_vE (b) and H (c), with the colors indicating the atmospheric boundary layer (ABL) stability. Highlighted by black circles are observations with a RH >80 %, where deposition through the external leaf path can still play an important role. The black crosses are observations from the fertilization event observed on 11 - 12 September.

Next, we organize the observations following current dynamic vegetation models, based on temperature, radiation and moisture (Jarvis et al., 1976; Stewart, 1988; Ronda et al., 2001). Here, we compare the responses of the four individual fluxes to temperature (T), PAR and VPD. As in the models these three variables control the stomatal response at canopy level, we will use the responses of the fluxes to these variables as a guidance to better understand the diurnal variability of the ammonia flux. Note that measurements taken on 11 - 12 September are not used to calculate correlation coefficients, but are shown in the figures and included in the visual analysis.

3.1 Relating the ammonia flux to photosynthesis

Plotting F_{NH_3} against the GPP in Fig. 4a shows a low positive correlation between the two fluxes, with a correlation coefficient of 0.48. There is a large spread in the data, particularly for GPP values larger than 0.125 mgC m^{-2}s^{-1}. Part of this spread is attributed to the high relative humidity (black circles), where F_{NH_3} is not yet dominated by stomatal exchange and the external leaf pathway is still expected to be significant. Note that the atmospheric stability (color coded) plays an important role for the GPP as unstable conditions are typically characterized by clear skies and high PAR values, which favors photosynthesis

(discussed in Section 3.2). This relation is not found in the observed F_{NH_3}, as there is a large spread in F_{NH_3} for both neutral and unstable conditions.

A moderate positive correlation is found in Fig. 4b between F_{NH_3} and L_vE. Our interpretation of this moderate correlation is that both ~~evaporation~~ transpiration and stomatal NH_3 emissions follow a similar process. The opening of the stomata for photosynthesis allows for the exchange of several gasses, including water vapor and ammonia, depending on VPD or the difference between atmosphere NH_3 and the stomatal compensation point (Cowan and Farquhar, 1977; Hsiao, 1973; Farquhar et al., 1980; Wichink Kruit et al., 2010). Note that L_vE represents the net ~~L_vE~~ evaporation (Miralles et al., 2020) since evaporation from the soil plays a role as well. Assuming a vegetation cover of 90% for grass, soil evaporation ~~could be between~~ contributes with estimations that range from 10 ~~and~~ to 30%. Despite this, the use of net L_vE is acceptable as an indicator for the transpiration process. Note further that the observations with high relative humidity generally correspond to low L_vE and that again unstable conditions correspond with high L_vE values, related to the VPD between the leaf and stomata, and the atmosphere.

When plotting F_{NH_3} against H, two branches are found in the spread of the data, with a third branch being formed by the filtered out fertilization event on 11 - 12 September (black crosses). The smaller branch, with $F_{NH_3} > 0.1$ μg m^{-2}s^{-1}, could point towards another (weaker) fertilization event. Still, the second highest positive correlation is found at 0.65, indicating that the natural diurnal variability indeed plays an important role. Note that most of the measurements with high relative humidity are clustered around H = 0 W m^{-2}, i.e. there is little transfer of heat between the surface and atmosphere.

Based on the three scatter plots we find the highest correlation between F_{NH_3} and L_vE. Together with the diurnal variability of F_{NH_3}, transitioning from nighttime deposition to daytime emission from 8:30 to 16:30 UTC, this is the second indication towards stomatal emission of NH_3, opposed to emission from fertilization or animal droppings. However, the moderate correlation between F_{NH_3} and H indicates that the diurnal variability of the fluxes influences the correlation coefficient. Finally, we want to mention the observations on 11 - 12 September, which support the interpretation of the scatter plots in showing how fertilization events affect our analysis.

3.2 The dynamic vegetation response to varying meteorological conditions

3.2.1 The dynamic response to temperature

We further investigate the stomatal exchange of NH_3 by analyzing the response of F_{NH_3} to varying meteorological conditions. The optimal conditions (PAR, T, VPD) for photosynthesis are different for different vegetation types (Gates, 1980; Jacobs, 1994; Vilà-Guerau de Arellano et al., 2015). Starting with the 2.8 meter temperature (T) in Fig. 5, we find a large spread for all four surface fluxes, resulting in low positive correlations (0.33 - 0.51). The lowest correlation coefficients are found for GPP and L_vE, indicating that temperature has little impact on the opening and closing of the stomata. Slightly higher correlation is found for F_{NH_3}, which we attribute to the relation between the stomatal compensation point and the NH_3 flux, discussed in Section 2.5. Note that the NH_3 emissions on 11 - 12 September stand out as outliers in Fig. 5a, while being average for the other three subplots.

3.2.2 The dynamic response to VPD

Moving on to analyzing the response of the four fluxes to the VPD, we find moderate correlation coefficients (0.42 - 0.53) in Fig. 6. L_vE shows in Fig. 6c a non-linear relationship with the VPD, called the evaporation hysteresis (Zhang et al., 2014; de Groot et al., 2019). This hysteresis is driven by both the vegetation regulating the loss of water through evaporation, described in Section 2.2, and the time difference when the maximum values for L_vE (12:00 UTC) and VPD (15:00 UTC) are reached. The same holds true for the other three fluxes (F_{NH_3}, GPP and H), as all three reach their maximum around noon.

Note that the observations of 11 - 12 September again are clear outliers in Fig. 6a, forming two branches in the scatter plot. Also standing out are several observations with $F_{NH_3} > 0.1$ μg m^{-2}s^{-1}. These are the observations that appear as the small upper branch in the H - F_{NH_3} scatter plot in Fig. 4c and, again, form their separate branch here in Fig. 6a. This further indicates that there is a second (weak) fertilization event in the filtered dataset of the RITA-2021 campaign.

3.2.3 The dynamic response to PAR

When relating ~~F_{NH_3}~~ the fluxes to PAR, we find high positive correlation coefficients for all four surface fluxes (0.72 - 0.93)~~in Fig. 7. The highest value is found for H~~ (Fig. 7~~d) , as the solar radiation is the main source of energy for the surface-atmosphere exchange of heat. Where H exhibits a linear relation to PAR, non-linear effects are observed in the response of the two photosynthesis fluxes GPP and L_vE. This difference, together with the high correlation coefficients, indicates~~) indicating that PAR is the main driver of the dynamic vegetation response.
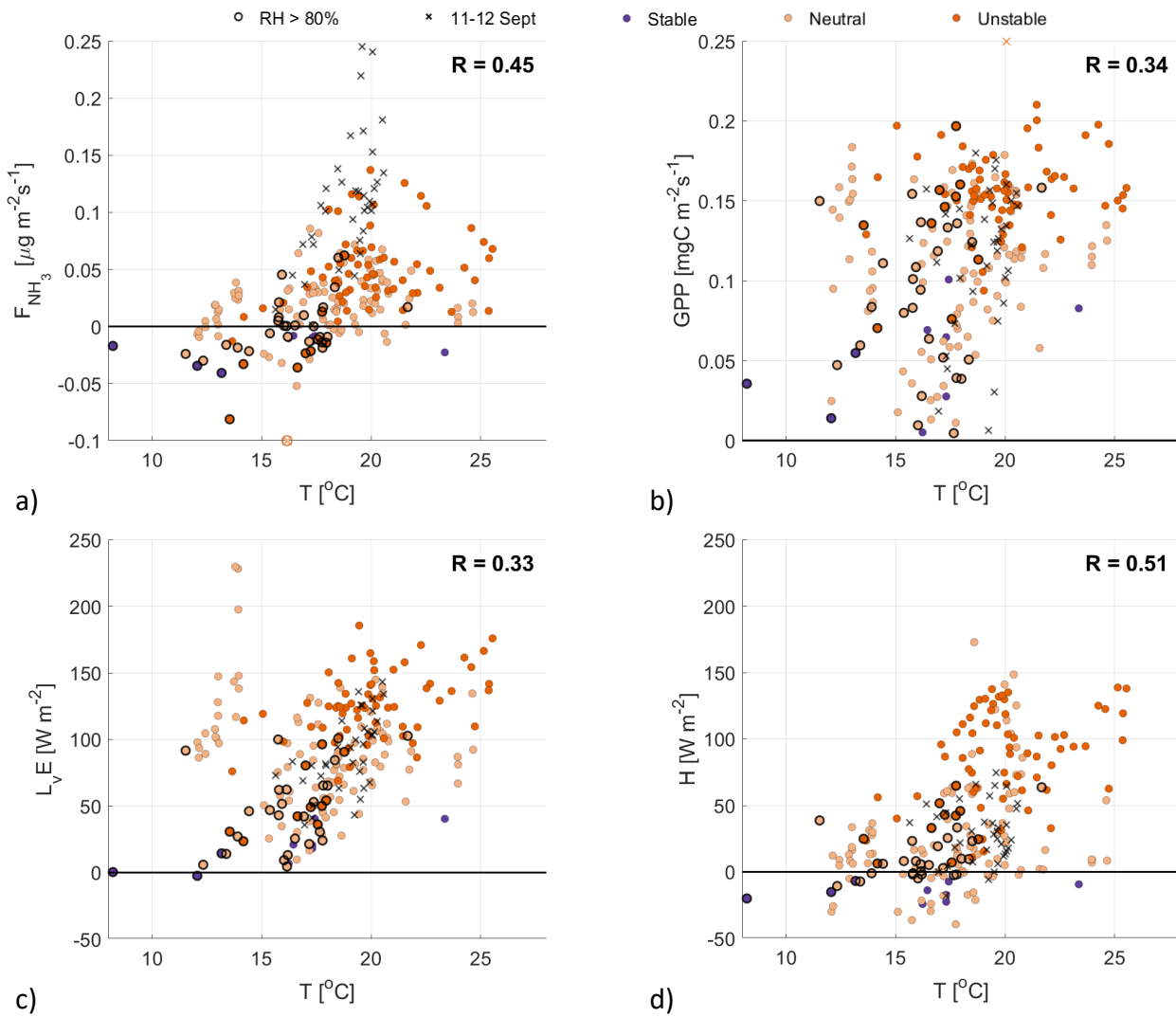
Figure 5. Scatter plots of the temperature against F_{NH_3} (a), GPP (b), L_vE (c) and H (d), with the colors indicating the ABL stability (see Figure 4 for legend). Highlighted by black circles are observations with a RH > 80 %. The black crosses are observations from the fertilization event on 11 - 12 September.
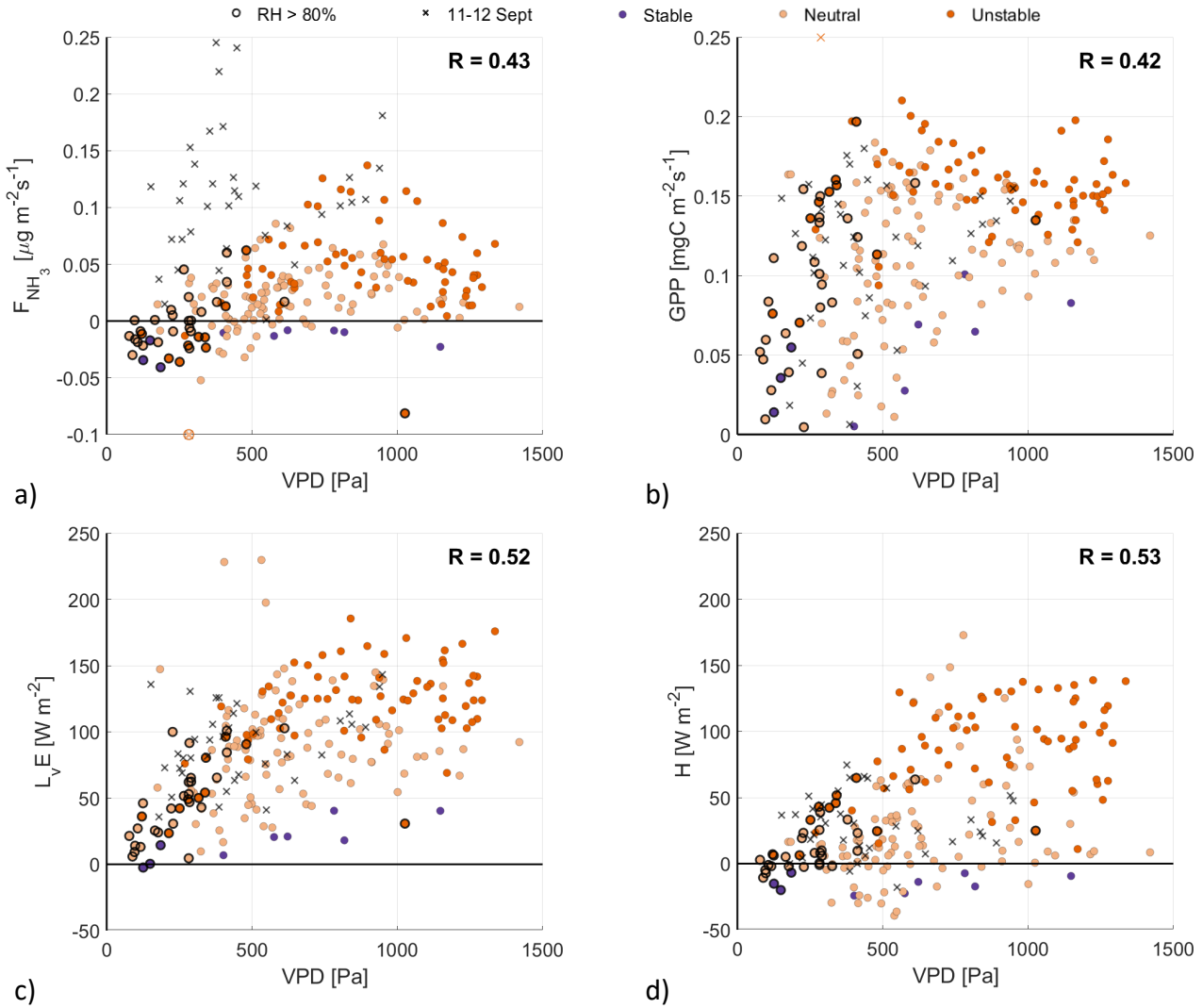
Figure 6. Scatter plots of the VPD against F_{NH_3} (a), GPP (b), L_vE (c) and H (d), with the colors indicating the ABL stability (see Figure 4 for legend). Highlighted by black circles are observations with a RH > 80 %. The black crosses are observations from the fertilization event on 11 - 12 September.
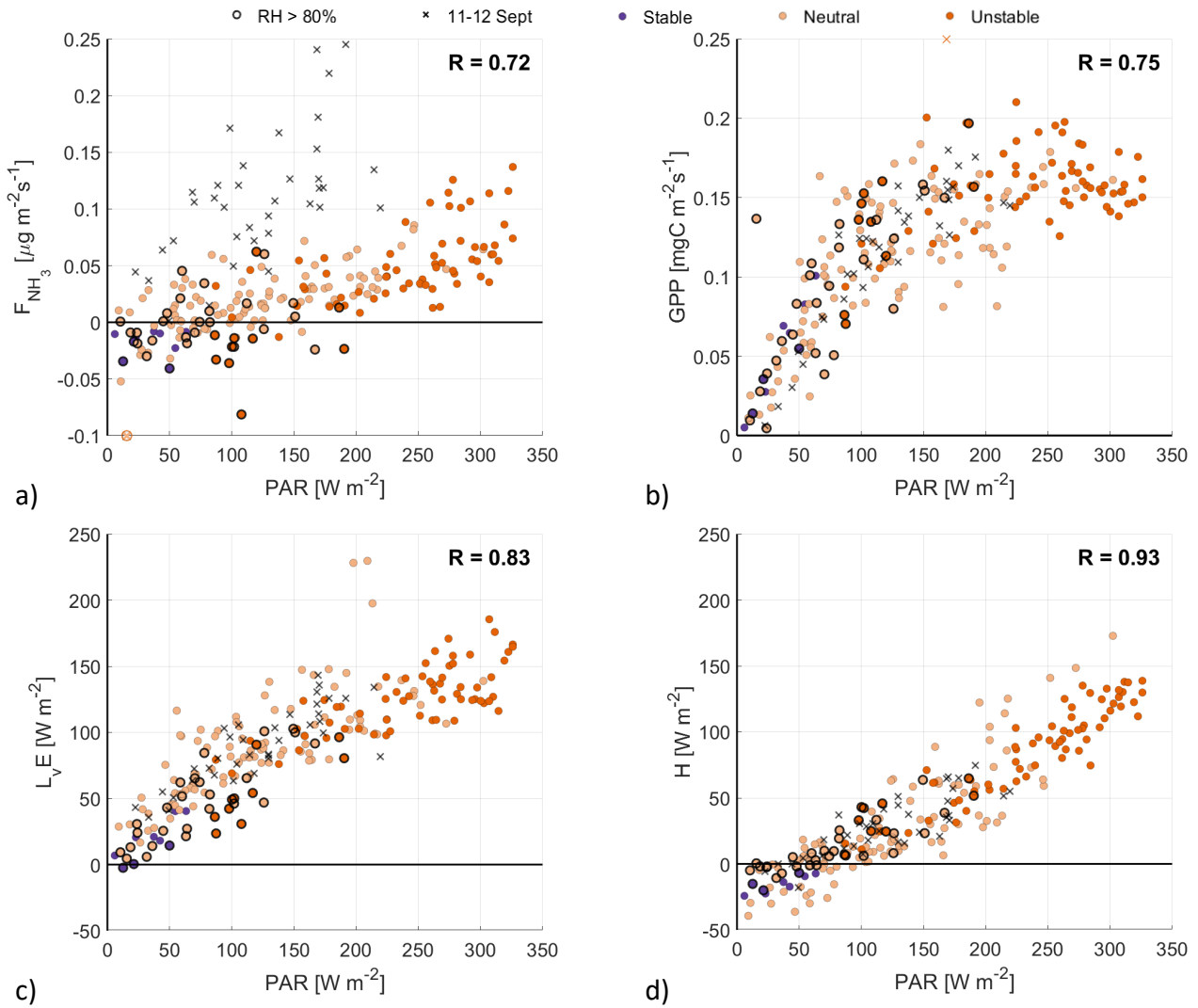
Figure 7. Scatter plots of PAR against F_{NH_3} (a), GPP (b), L_vE (c) and H (d), with the colors indicating the ABL stability (see Figure 4 for legend). Highlighted by black circles are observations with a RH > 80 %. The black crosses are observations from the fertilization event on 11 - 12 September.

The GPP has a strongly non-linear response to PAR, as the GPP appears to reach a plateau for PAR > 150 W m^{-2}. There are several reasons for this GPP maximum. At constant temperature and PAR, the stomatal uptake of CO$_2$ will increase the concentration within the plant to the point that the CO$_2$ supply is no longer the limiting factor. The GPP then reaches a plateau of maximum photosynthesis rate (see Figure 6.13a Moene and Van Dam (2014)), similar to the observations in Fig. 7b.

5 Additionally, the photosynthesis system can become light saturated for high PAR values, at constant temperature. Following this latter process, the GPP is expected to level off more gradually, compared to the plateau that is reached by CO$_2$ saturation (see Figure 6.13b Moene and Van Dam (2014)). Finally, the (partly) closing of the stomata in response to high VPD could also reduce the GPP. However, as the VPD typically reaches its maximum around 15:00 UTC (not shown), it is unlikely that this is a limiting factor for GPP at high PAR values, which peaks around noon. All these processes depend on the temperature, VPD

10 and PAR, and can explain the vertical spread in Fig. 7b.

When taking a close look at the response of ~~the~~ L$_v$E to PAR, ~~is it~~ it is possible to distinguish two phases in Fig. 7c. First, for PAR values up to about 100 W m^{-2}, ~~the~~ L$_v$E increases linearly to roughly 75 W m^{-2}, related to the opening/closing of the stomata around sunrise/sunset. The second phase shows a more gradual linear increase of L$_v$E to PAR. From the linear response and the small spread in Fig. 7c, we conclude that opening and closing of the stomata during the RITA-2021 campaign

15 is governed by PAR and that the role of the VPD or temperature is small.

Similar to ~~the~~ L$_v$E, the NH$_3$ flux generally shows a linear response; transitioning from weak deposition to emission as the stomata open in response to increasing PAR. The spread in the F$_{NH_3}$ response is larger compared to the L$_v$E response, which results in the lowest correlation coefficient at 0.72. We attribute this spread to three factors: the relation between temperature and the stomatal compensation point, the variations in the NH$_3$ concentration and the measurements where RH > 80 % (black

20 circles). Furthermore, observations where F$_{NH_3}$ > 0.1 μg m^{-2}s^{-1}, i.e. the possible (weak) fertilization event, again appear to form a second branch in the scatter plot. Based on the strong similarities between F$_{NH_3}$ and L$_v$E in their response to PAR, we ~~conclude that~~ interpret the observed NH$_3$ emission ~~is indeed~~ as stomatal (re)emission from vegetation.

4 Discussion

Observations of the NH$_3$ flux after filtering, taken over 17 individual days during the RITA-2021 campaign, are characterized

25 by day-time emissions. The measurement site at Cabauw is located on flat grassland in an agricultural area, with the nearby fields being actively managed and/or grazed upon. It is therefore possible that the observed NH$_3$ emissions originate from sources like fertilization events (e.g. manure application) or animal droppings. ~~We therefore first aim to establish relationships between the NH$_3$ emissions to stomatal exchange and follow up by attempting to find relations between F~~Clearly distinguishing between stomatal driven emission and volatilization of ammonia due to fertilization events is complex due to the contributions

30 of different paths (soil versus plant) and non-linear effects (water vapor deficit dependence on temperature) that often offset each other. However, we identified F$_{NH_3}$ ~~and observations of the CO$_2$ and water vapor flux.~~ which are most likely due to a fertilization event and labeled these data as outliers, while keeping other doubtful points in the analysis. Next, we also marked F$_{NH_3}$ which could be due to exchange via the external pathway, once more trying to single out F$_{NH_3}$ due to stomatal exchange. ~~The first indication~~

35 Indications towards stomatal emission is found in the diurnal variability of F$_{NH_3}$. The flux transitions from deposition to emission in the early morning around 8:00 UTC, reaches maximum emission around 12:00 UTC and transitions to deposition again just before sunset, around 16:30 UTC, as shown in Fig. 2c. Our interpretation of this diurnal cycle is the flux transitions from (nighttime) NH$_3$ deposition, through the external leaf path, towards emission through the stomatal path during the day. This diurnal variability of F$_{NH_3}$ shares similarities to the diurnal variability of the CO$_2$ flux. As the stomata open for photosyn-

40 thesis in response to PAR, the CO$_2$ flux transitions from CO$_2$ respiration to stomatal uptake of CO$_2$. High correlation between F$_{NH_3}$ and L$_v$E (0.7) and between F$_{NH_3}$ and PAR (0.72), further point towards stomatal NH$_3$ emission and a possible relation between F$_{NH_3}$ and the photosynthesis fluxes.

4.1 Critical analysis of RITA-2021 dataset

The conditions during the RITA-2021 campaign present a challenge for the analysis conducted in this study. The site is located

45 in an active agricultural region, with several potential emission sources within only a few hundred meters to a couple of kilometers distance upwind of the measurement site. The fields next to the site are actively managed and nitrogen contents of the soil and vegetation can differ on a field-to-field basis. This high level of surface heterogeneity within the estimated footprint of the flux measurements (up to about 250 m, Table 2) adds an additional level of complexity to the analysis (Swart et al., 2023). Furthermore, there are several farms located within two kilometers of the site, some of which with yearly NH$_3$

50 emissions up to ~~12000~~ 1200 kg year^{-1}. Studies on the blending distance (i.e. the distance at which a plume can be considered

well-mixed with respect to the background) indicate that emission plumes from such strong local NH$_3$ sources can affect flux measurements over distances of a couple of kilometers (Schulte et al., 2022). In this study, at least one instance of strong local emissions has been identified as the fertilization event on 11 - 12 September. Other potential weaker events have been shown and discussed as well in Fig. 4a, 4c and 6a.

The analysis is further complicated by the complex meteorological conditions, characterized by frontal passages. As the miniDOAS setup was positioned anticipating winds from the south-west, the meteorology of the filtered data is characterized by frontal passages. As a result, most observations are taken under neutral stability conditions (60 %), with clouds and some rain showers. While rain events are filtered out, wet deposition by rain does lead to a sudden change in the NH$_3$ concentration and can lead to re-emission of NH$_3$ as the rainwater evaporates.

Finally, the south-western orientation of the instruments leads to a significant loss in the availability of data suitable for analysis. Historically, southwestern winds tend to be most common in September, but the wind direction during the campaign was highly variable. Filtering for unobstructed wind directions reduces the availability of viable data by 510 hours, i.e. 44 % of all measurement data. As a result, the observed range in the measurements presented in the Figures is strongly influenced by the natural diurnal variability of the variables. While we do address the role of the natural diurnal variability by including the sensible heat flux in our analysis, it does make the observed relations between F$_{NH_3}$ and the other variables somewhat speculative.

The high level of heterogeneity due to complex emission sources, the low data availability after filtering and the complex weather conditions make the RITA-2021 dataset unfavorable for establishing relationships between F$_{NH_3}$ and the CO$_2$ or water vapor flux. It also makes the dataset unsuitable to aid annual inventories. Yet, it highlights the importance of homogeneity of the NH$_3$ surface characteristics and that proximity of NH$_3$ emission sources should be considered as well when selecting a measurement site, in addition to the availability of high quality meteorological observations. Despite the challenges, the NH$_3$ measurements are of unprecedented high quality (Swart et al., 2023) and analyzing the unique dataset following our approach is still worthwhile. While we do not manage to develop new relationships , we are able to link the observed F$_{NH_3}$ emission to stomatal exchange, following an approach where we organize the observations following ; establishing relationships that significantly correlate with the main drivers of the stomatal aperture following current dynamic vegetation models.

4.2   Recommendations

Following the results presented in this study, we recommend a comprehensive approach to future NH$_3$ flux measurements, including observations of the CO$_2$ and water vapor flux as auxiliary measurements. The opening of the stomata for CO$_2$ uptake through photosynthesis allows for the exchange of several other gasses, including water vapor and ammonia. The process representations of photosynthesis have been widely researched and it has been better tested against sub-diurnal observations under different scales (Vilà-Guerau de Arellano et al., 2020) and such auxiliary observations can be used to further our understanding of NH$_3$ exchange through the individual exchange pathways, as was done for ozone deposition by Visser et al. (2021).

Furthermore, we recommend to analyze and compare observations of the NH$_3$ flux at different measurement (grassland) sites, similar to the intercomparison of CO$_2$ exchange measurements by Jacobs et al. (2007). For example, the F$_{NH_3}$ diurnal variability presented in this study significantly differs from measurements in 2013 at the Veenkampen meteorological site near the city of Wageningen (https://www.wur.nl/en/show/Weather-Station-De-Veenkampen.htm). Located only 50 km east, the diurnal variability of F$_{NH_3}$ at Veenkampen is characterized by weak morning deposition and strong afternoon deposition, up to about -0.3 μg m^{-2}s^{-1}, for clear sky conditions over unfertilized grassland (Schulte et al., 2021). At the Haarweg meteorological site, the predecessor to the Veenkampen, chemical wet denuder measurements of F$_{NH_3}$ in 2004 were characterized by strong deposition in the early morning, attributed to morning dew, and weak stomatal emissions in the afternoon (Wichink Kruit et al., 2007). The differences between observed diurnal variability in these three studies stress the high variability at the local and regional scales and highlight the need for long term high-resolution F$_{NH_3}$ observations at multiple locations.

Efforts to further our understanding of the NH$_3$ exchange and its diurnal variability are already being made. The miniDOAS setup used in the RITA-2021 will be taking long-term (> 1 year) observations of the NH$_3$ flux at the Veenkampen meteorological site, starting in the spring of 2023. This year-long record of high-resolution F$_{NH_3}$ observations will be analyzed, alongside a wide range of meteorological and turbulent measurements, including the CO$_2$ and water vapor flux, aiming to improve the parameterization of the NH$_3$ surface-atmosphere exchange. The collocation of surface and upper-atmospheric observations (Vilà-Guerau de Arellano et al., 2023) is key to obtain a comprehensive and complete understanding of NH$_3$ flux. The analysis can be taken one step further in the context of the Ruisdael Observatory project, following a process analysis combining the observations with both conceptual (Schulte et al., 2021) and high-resolution turbulent resolved models (Schulte et al., 2022).

5   Conclusions

We ~~analyze~~ analyzed over a month of ammonia flux measurements (F$_{NH_3}$), taken during the RITA-2021 campaign at the Ruisdael Observatory at Cabauw. The analysis is centered around observations from the miniDOAS flux measurement setup, which applies the flux-gradient method to line average concentration measurements over a 22 m open-path at two heights. Our objective was to find relationships between the observed NH$_3$ flux and the ~~other turbulent surface fluxes such as sensible heat flux and photosynthesis, i.e. the stomatal exchange of CO$_2$ and water vapor (plant transpiration).~~ main drivers of dynamic vegetation response, linking ammonia exchange through the main three variables that control the stomatal pathway to processes due to photosynthesis. The process of photosynthesis has been more widely studied and ~~such auxiliary observations can be used to advance our understanding of NH$_3$ surface-atmosphere exchange through the individual exchange pathways, e.g. stomatal exchange.~~ therefore establishing robust relationships between photosynthesis drivers closely linked to stomatal aperture and NH3 surface exchange enable us to determine and quantify the role of this path in emiting or depositing ammonia.

After filtering, the observed F$_{NH_3}$ is characterized by daytime emissions, averaging at about 0.05 μg m^{-2}s^{-1}, and nighttime deposition of about -0.05 μg m^{-2}s^{-1}. We compare the NH$_3$ flux to the from observations inferred CO$_2$ uptake by vegetation and the net observed exchange of water vapor, represented by the gross primary production (GPP) and net latent heat flux (L$_v$E), as well as the sensible heat flux (H) which is only indirectly related to the dynamic vegetation response. Here, we find high and significant correlation between the observed daytime NH$_3$ emissions and L$_v$E (0.70) and the photosynthetically active radiation (PAR, 0.72). These results provide a first-order quantification of ~~stomatal emission of NH$_3$~~ how NH$_3$ exchange could follow similar paths as the exchange of CO$_2$ and H$_2$O through plant processes regulated by the stomatal aperture.~~.~~ It shows that auxiliary and collocated flux measurements of CO$_2$ and water vapor are appropriate variables to distinguish stomatal NH$_3$ exchange from non-stomatal exchange.

The analysis presented in this study is hampered by the challenging conditions during the RITA-2021 campaign. ~~The measurement site is located in a highly agricultural region, with actively managed (i.e. fertilized) grassland and emission sources in close proximity (< 2 km) of the NH$_3$ measurements. These heterogeneous NH$_3$ surface characteristics lead to outlier observations caused by at least one fertilization event and there are indications of other (weaker) fertilization events. Additional layers of complexity are added by the varying meteorological conditions, characterized by frontal passages, and the small subset of the campaign measurements being suitable for analysis after filtering (9 % or 102 hours). The latter is largely the outcome of filtering out unfavorable wind directions, where the airflow is obstructed. As a result, the observed range in the measurements is largely governed by the natural diurnal variability, hampering the efforts to establish clear relationships.~~

~~Despite the challenging conditions, the~~ However, despite these conditions, the comprehensive approach presented in this study paves the way for the potential of combining high-quality NH$_3$ observations with auxiliary flux measurements of CO$_2$, water vapor and other meteorological variables. By organizing ~~the observations following current dynamic vegetation models~~ and analyzing the observations guided and constrained by the main meteorological drivers controlling the assimilation and transpiration in grass fields, we managed to attribute the observed NH$_3$ emission to processes and variables associated to stomatal exchange and identify outliers. In order to establish ~~relations between the~~ more robust relations between NH$_3$ and the photosynthesis fluxes, the ~~approach~~ proposed framework in this study should be applied to measurements that are still representative of the nearby sources and sinks, but ~~at the same time are well mixed and outside the blending distance of nearby emission sources .~~ insuring a blending distance that guarantees that these singular sources and sinks contributions are properly mixed with the NH$_3$-background concentration. These distances range from 1000 m to 3000 m (Schulte et al., 2022). Further, longer time series are needed in order to make a ~~better~~ more robust distinction between days with and without the influences of nearby sources. Our findings and framework over grasslands are a first step to confirm patterns and relationships between meteorological drivers and NH$_3$ exchange, but should be extended to longer and more dedicated field campaigns, including other ecosystems. The results presented in this study already indicate that there is room to find such patterns.

Author Contributions

RS: Conceptualization, Formal Analysis, Investigation, Methodology, Visualization, Writing - original draft preparation. JVGdA: Conceptualization, Writing - Review and Editing, Supervision~~MCvZ: Conceptualization, Funding Acquisition, Writing - Review and Editing. JZ: Investigation (CO~~ SJR: Methodology and Investigation (NH$_{23}$ flux ~~and meteorological data) . SvdG and SJR~~ data) SvdG Investigation (NH$_3$ flux data). JZ: Investigation (CO$_2$ flux and meteorological data). MCvZ: Conceptualization, Funding Acquisition, Writing - Review and Editing.
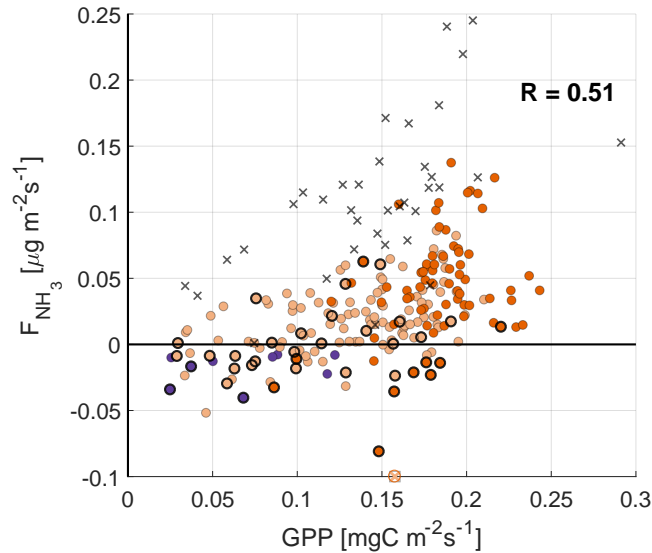
Figure A1. Scatter plots of F_{NH_3} against the GPP, with the colors indicating the atmospheric boundary layer (ABL) stability. Highlighted by black circles are observations with a RH >80 %, where deposition through the external leaf path can still play an important role. The black crosses are observations from the fertilization event observed on 11 - 12 September.

Competing interests

The authors declare that they have no conflict of interest.

Appendix A: An alternative way of calculating ecosystem respiration

In 2.2, we describe our approach to arrive at an estimate of GPP using observations only. Here, we examine the potential impact of using a regression model to describe the ecosystem respiration to examine the potential impact of using a different method on the results. We calculated GPP by describing ecosystem respiration as a function of air temperature using the exponential regression model of Lloyd and Taylor (1994), hereafter LT94:

$$ER = R_{10}exp(E_0(\frac{1}{T_{\text{ref}} - T_0} - \frac{1}{T - T_0}) \tag{A1}$$

Where R_{10} is the reference respiration at reference temperature T_{ref} (set to 10 °C). To avoid over-paramaterisation, T_0 is set to -46.02 °C, as in LT94. E_0 is an empirical parameter related to the activation energy. Using the night-time data collected during the campaign, filtered for $u_* > 0.1ms^{-1}$, and quality flag of 0 (Mauder and Foken, 2006), we obtained values of 5.3 for R_{10}, and 124 for E_0. In doing so, correlation coefficients for the corresponding panels in Figure 4 -3.2.3 of the main text slightly improved. Figures A1 - A4 show the scatter plots, using this alternative formulation of GPP.

Acknowledgements. Ruben B. Schulte PhD project was supported by RIVM within the framework of project 36.7: Monitoring of dry ammonia deposition; financed by the Dutch Ministry of Agriculture, Nature and Food Quality. We thank the Royal Netherlands Meteorological Institute (KNMI) for site access and assistance during the RITA -2021 campaign. All ~~people of RIVM and TNO~~ our colleagues of RIVM (D. Swart, S. Berkhout, R. van der Hoff and M. Haaima) and of TNO (A. Hensen, P. Wintjen, A. Frumau and P. van den Bulk) involved in this campaign are gratefully acknowledged for their support, dedicated work to make the campaign a success and fruitful discussions during the analysis of the data. This article has been accomplished by using data generated in the Ruisdael Observatory, a scientific research infrastructure which is (partly) financed by the Dutch Research Council (NWO, grant number 184.034.015).
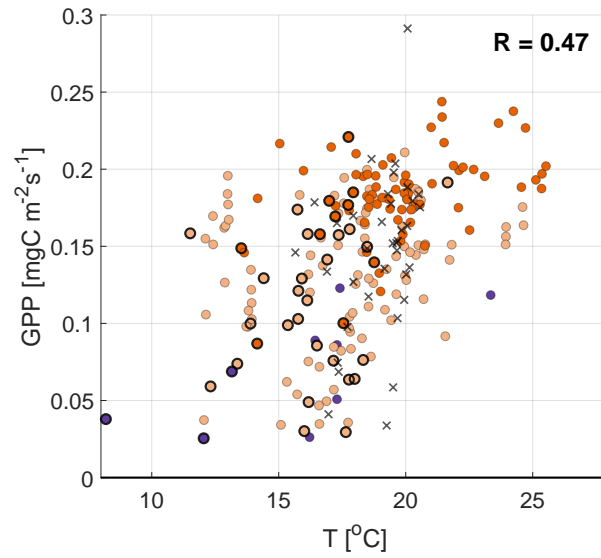
Figure A2. Scatter plots of the temperature GPP, with the colors indicating the ABL stability (see Figure 4 for legend). Highlighted by black circles are observations with a RH > 80 %. The black crosses are observations from the fertilization event on 11 - 12 September.
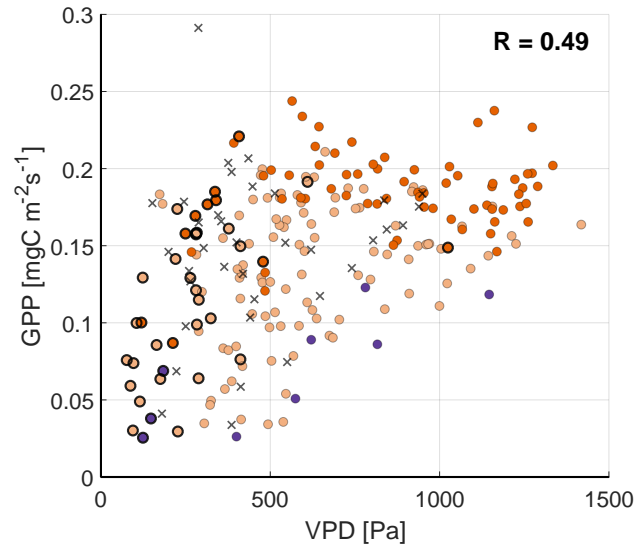
Figure A3. Scatter plots of the VPD against GPP, with the colors indicating the ABL stability (see Figure 4 for legend). Highlighted by black circles are observations with a RH > 80 %. The black crosses are observations from the fertilization event on 11 - 12 September.
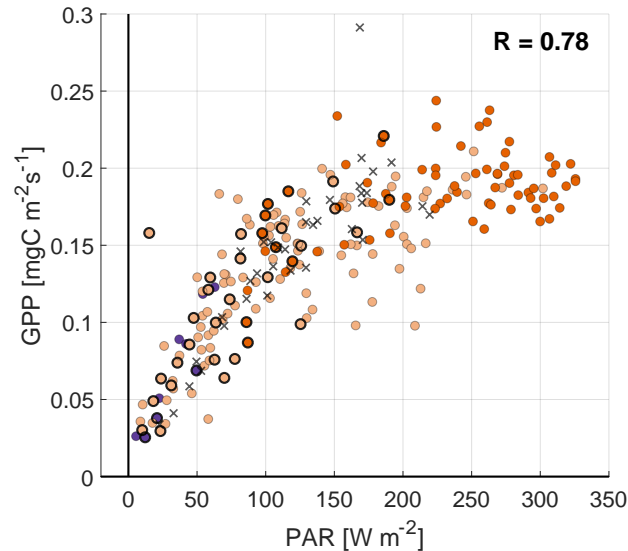
Figure A4. Scatter plots of PAR against GPP, with the colors indicating the ABL stability (see Figure 4 for legend). Highlighted by black circles are observations with a RH > 80 %. The black crosses are observations from the fertilization event on 11 - 12 September.

References

Behera, S. N., Sharma, M., Aneja, V. P., and Balasubramanian, R.: Ammonia in the atmosphere: a review on emission sources, atmospheric chemistry and deposition on terrestrial bodies, Environmental Science and Pollution Researc, 20, 8092 – 8131, https://doi.org/10.1007/s11356-013-2051-9, 2013.

Berkhout, A. J. C., Swart, D. P. J., Volten, H., Gast, L. F. L., Haaima, M., Verboom, H., Stefess, G., Hafkenscheid, T., and Hoogerbrugge, R.: Replacing the AMOR with the miniDOAS in the ammonia monitoring network in the Netherlands, Atmospheric Measurement Techniques, 10, 4099–4120, https://doi.org/10.5194/amt-10-4099-2017, 2017.

Bobbink, R., Hornung, M., and Roelofs, J. G. M.: The effects of air-borne nitrogen pollutants on species diversity in natural and semi-natural European vegetation, Journal of Ecology, 86, 717 – 738, https://doi.org/10.1046/j.1365-2745.1998.8650717.x, 2003.

Bosveld, F., Baas, P., Beljaars, A., Holtslag, A., Vilà-Guerau de Arellano, J., and van de Wiel, B.: Fifty Years of Atmospheric Boundary-Layer Research at Cabauw Serving Weather, Air Quality and Climate, Boundary-Layer Meteorology, 177, 583–612, https://doi.org/10.1007/s10546-020-00541-w, 2020.

Brauer, C. C., Torfs, P. J. J. F., Teuling, A. J., and Uijlenhoet, R.: The Wageningen Lowland Runoff Simulator (WALRUS): application to the Hupsel Brook catchment and the Cabauw polder, Hydrology and Earth System Sciences, 18, 4007–4028, https://doi.org/10.5194/hess-18-4007-2014, 2014.

Cowan, I. and Farquhar, G.: Stomatal function in relation to leaf metabolism and environment, Camebridge: at the university press, pp. 471 – 505, 1977.

de Groot, G. E., Vilà-Guerau de Arellano, J., de Roode, S. R., Coenders-Gerrits, A. M. J., and van de Wiel, B. J. H.: Evaporation Hysteresis over Vegetation: The Impact of Surface Processes and Boundary Layer Dynamics, Master's thesis, Delft University of Technology, the Netherlands, http://resolver.tudelft.nl/uuid:8284f137-2c64-48ab-ba8d-bf099d70c70c, 2019.

Erisman, J. and Schaap, M.: The need for ammonia abatement with respect to secondary PM reductions in Europe, Environmental Pollution, 129, 159–163, https://doi.org/10.1016/j.envpol.2003.08.042, 2004.

Erisman, J. W., Galloway, J. N., Seitzinger, S., Bleeker, A., Dise, N. B., Petrescu, A. M. R., Leach, A. M., and de Vries, W.: Consequences of human modification of the global nitrogen cycle, Philosophical Transactions of the Royal Society B: Biological Sciences, 368, 20130 116, https://doi.org/10.1098/rstb.2013.0116, 2013.

Farquhar, G. D., Firth, P. M., Wetselaar, R., and Weir, B.: On the Gaseous Exchange of Ammonia between Leaves and the Environment: Determination of the Ammonia Compensation Point, Plant Physiology, 66, 710–714, https://doi.org/10.1104/pp.66.4.710, 1980.

Ferrara, R., Di Tommasi, P., Famulari, D., and Rana, G.: Limitations of an Eddy-Covariance System in Measuring Low Ammonia Fluxes, Boundary-Layer Meteorology, 180, 173–186, https://doi.org/10.1007/s10546-021-00612-6, 2021.

Gates, D. M.: Biophysical ecology, Springer-Verlag, 1980.

Hsiao, T.: Plant responses to water stress, Annu. Rev. Plant Physiol., 24, 519–570, 1973.

Jacobs, C.: Direct impact of atmospheric CO2 enrichment on regional transpiration, Ph.D. thesis, Wageningen University, https://wur.on. worldcat.org/oclc/906644518, 1994.

Jacobs, C. M. J. and de Bruin, H. A. R.: Predicting Regional Transpiration at Elevated Atmospheric CO2: Influence of the PBL–Vegetation Interaction, Journal of Applied Meteorology, 36, 1663 – 1675, https://doi.org/10.1175/1520-0450(1997)036<1663:PRTAEA>2.0.CO;2, 1997.

Jacobs, C. M. J., Jacobs, A. F. G., Bosveld, F. C., Hendriks, D. M. D., Hensen, A., Kroon, P. S., Moors, E. J., Nol, L., Schrier-Uijl, A., and Veenendaal, E. M.: Variability of annual CO_2 exchange from Dutch grasslands, Biogeosciences, 4, 803–816, https://doi.org/10.5194/bg-4-803-2007, 2007.

Jarvis, P. G., Monteith, J. L., and Weatherley, P. E.: The interpretation of the variations in leaf water potential and stomatal conductance found in canopies in the field, Philosophical Transactions of the Royal Society of London. B, Biological Sciences, 273, 593–610, https://doi.org/10.1098/rstb.1976.0035, 1976.

Kljun, N., Calanca, P., Rotach, M. W., and Schmid, H. P.: A simple two-dimensional parameterisation for Flux Footprint Prediction (FFP), Geoscientific Model Development, 8, 3695–3713, https://doi.org/10.5194/gmd-8-3695-2015, 2015.

Lloyd, J. and Taylor, J.: On the temperature dependence of soil respiration, Functional Ecology, 8, 315–323, https://doi.org/10.2307/2389824, 1994.

Massad, R.-S., Nemitz, E., and Sutton, M. A.: Review and parameterisation of bi-directional ammonia exchange between vegetation and the atmosphere, Atmospheric Chemistry and Physics, 10, 10 359–10 386, https://doi.org/10.5194/acp-10-10359-2010, 2010.

Mauder, M. and Foken, T.: Impact of post-field data processing on eddy covariance flux estimates and energy balance closure, Meteorologische Zeitschrift, 15, 597–609, https://doi.org/10.1127/0941-2948/2006/0167, 2006.

Mauder, M., Foken, T., Aubinet, M., and Ibrom, A.: Eddy-covariance measurements. Ch. in Springer Handbook of Atmospheric Measurements, Springer International Publishing, https://doi.org/https://doi.org/10.1007/978-3-030-52171-4, 2022.

McDermitt, D. K., Burba, G., Xu, L., Anderson, T. G., Komissarov, A. V., Riensche, B., Schedlbauer, J. L., Starr, G., Zona, D., Oechel, W. C., Oberbauer, S. F., and Hastings, S. J.: A new low-power, open-path instrument for measuringmethane flux by eddy covariance, Appl. Phys. B, 102, 391–405, https://doi.org/https://doi.org/10.1007/s00340-010-4307-0, 2011.

Milford, C., Hargreaves, K. J., Sutton, M. A., Loubet, B., and Cellier, P.: Fluxes of NH3 and CO2 over upland moorland in the vicinity of agricultural land, Journal of Geophysical Research: Atmospheres, 106, 24 169–24 181, https://doi.org/10.1029/2001JD900082, 2001.

Miralles, D. G., Brutsaert, W., Dolman, A. J., and Gash, J. H.: On the use of the term 'evapotranspiration', Water Resources Research, 56, https://doi.org/10.1029/2020WR028055, 2020.

Moene, A. F. and Van Dam, J. C.: Transport in the Atmosphere-Vegetation-Soil Continuum, Camebridge University Press, 2014.

Moncrieff, J., Massheder, J., Bruin de, H., Ebers, J., Friborg, T., Heusinkveld, B., Kabat, P., Scott, S., Soegaard, H., and Verhoef, A.: A system to measure surface fluxes of momentum, sensible heat, water vapor and carbon dioxide., Journal of Hydrology, 188-189, 589–611, 1997.

Moncrieff, J., Clement, R., Finnigan, J., and Meyers, T.: Averaging, detrending and filtering of eddy covariance time series, Ch. in Handbook of micrometeorology: a guide for surface flux measurements, Kluwer Academic, https://doi.org/https://doi.org/10.1007/1-4020-2265-4, 2004.

Nemitz, E., Milford, C., and Sutton, M.: A two-layer canopy compensation point model for describing bi-directional biosphere-atmosphere exchange of ammonia, Quarterly Journal of the Royal Meteorological Society, 127, 815–833, https://doi.org/10.1002/qj.49712757306, 2001.

Nemitz, E., Sutton, M., Wyers, G., and Jongejan, P.: Gas-particle interactions above a Dutch heathland: I. Surface exchange fluxes of NH 3, SO 2, HNO 3 and HCl, Atmospheric Chemistry and Physics, 4, 989–1005, https://doi.org/10.5194/acp-4-989-2004, 2004.

Papaioannou, G., Nikolidakis, G., Asimakopoulos, D., and Retalis, D.: Photosynthetically active radiation in Athens, Agricultural and Forest Meteorology, 81, 287–298, https://doi.org/10.1016/0168-1923(95)02290-2, 1996.

Parrish, D. D. and Fehsenfeld, F. C.: Methods for gas-phase measurements of ozone, ozone precursors and aerosol precursors, Atmospheric Environment, 34, 1921–1957, https://doi.org/10.1016/S1352-2310(99)00454-9, 2000.

RIVM, CBS, PBL, and WUR: Nitrogen deposition, 1990-2018, Available at https://www.clo.nl/indicatoren/en018918, (Indicator 0189, version 18 , 25 November 2019) RIVM National Institute for Public Health and the Environment, Bilthoven; Statistics Netherlands (CBS), The Hague; PBL Netherlands Environmental Assessment Agency, The Hague; and Wageningen University and Research, Wageningen. (Last access: 17 August 2022), 2019.

Ronda, R. J., de Bruin, H. A. R., and Holtslag, A. A. M.: Representation of the Canopy Conductance in Modeling the Surface Energy Budget for Low Vegetation, Journal of Applied Meteorology, 40, 1431–1444, https://doi.org/10.1175/1520-0450(2001)040<1431:ROTCCI>2.0.CO;2, 2001.

San José, J. J., Montes, R., and Nikonova-Crespo, N.: Carbon Dioxide and Ammonia Exchange in the Trachypogon Savannas of the Orinoco Llanos, Annals of Botany, 68, 321–328, https://doi.org/10.1093/oxfordjournals.aob.a088259, 1991.

Schrader, F., Erisman, J. W., and Brümmer, C.: Towards a coupled paradigm of NH3-CO2 biosphere–atmosphere exchange modelling, Global Change Biology, 26, 4654–4663, https://doi.org/10.1111/gcb.15184, 2020.

Schulte, R., van Zanten, M., Rutledge-Jonker, S., Swart, D., Wichink Kruit, R., Krol, M., van Pul, W., and Vilà-Guerau de Arellano, J.: Unraveling the diurnal atmospheric ammonia budget of a prototypical convective boundary layer, Atmospheric Environment, 249, 118 153, https://doi.org/10.1016/j.atmosenv.2020.118153, 2021.

Schulte, R. B., van Zanten, M. C., van Stratum, B. J. H., and Vilà-Guerau de Arellano, J.: Assessing the representativity of NH$_3$ measurements influenced by boundary-layer dynamics and the turbulent dispersion of a nearby emission source, Atmospheric Chemistry and Physics, 22, 8241–8257, https://doi.org/10.5194/acp-22-8241-2022, 2022.

Smit, L. A. M. and Heederik, D.: Impacts of Intensive Livestock Production on Human Health in Densely Populated Regions, GeoHealth, 1, 272–277, https://doi.org/10.1002/2017GH000103, 2017.

Stewart, J.: Modelling surface conductance of pine forest, Agricultural and Forest Meteorology, 43, 19–35, https://doi.org/10.1016/0168-1923(88)90003-2, 1988.

Stokstad, E.: Nitrogen crisis threatens Dutch environment- and economy, Science, 366, 1180–1181, https://doi.org/10.1126/science.366.6470.1180, 2019.

Swart, D., Zhang, J., van der Graaf, S., Rutledge-Jonker, S., Hensen, A., Berkhout, S., Wintjen, P., van der Hoff, R., Haaima, M., Frumau, A., van den Bulk, P., Schulte, R., van Zanten, M. C., and van Goethem, T.: Field comparison of two novel open-path instruments that measure dry deposition and emission of ammonia using flux-gradient and eddy covariance methods, Atmospheric Measurement Technique, 2023, 529–546, https://doi.org/10.5194/amt-16-529-2023, 2023.

Takagi, K., Tsuboya, T., and Takahashi, H.: Diurnal hystereses of stomatal and bulk surface conductances in relation to vapor pressure deficit in a cool-temperate wetland, Agricultural and Forest Meteorology, 91, 177–191, https://doi.org/10.1016/S0168-1923(98)00078-1, 1998.

Van Hove, L., Adema, E., Vredenberg, W., and Pieters, G.: A study of the adsorption of NH3 and SO2 on leaf surfaces, Atmospheric Environment (1967), 23, 1479–1486, https://doi.org/10.1016/0004-6981(89)90407-1, 1989.

van Zanten, M. C., Sauter, F. J., Wichink Kruit, R. J., van Jaarsveld, J. A., and van Pul, W. A. J.: Description of the DEPAC module: Dry deposition modelling with DEPAC-GCN2010, Tech. Rep. 680180001, National Institute for Public Health and the Environment (RIVM), https://www.rivm.nl/bibliotheek/rapporten/680180001.pdf, 2010.

Vilà-Guerau de Arellano, J., Ney, P., Hartogensis, O., de Boer, H., van Diepen, K., Emin, D., de Groot, G., Klosterhalfen, A., Langensiepen, M., Matveeva, M., Miranda-García, G., Moene, A. F., Rascher, U., Röckmann, T., Adnew, G., Brüggemann, N., Rothfuss, Y., and Graf, A.: CloudRoots: integration of advanced instrumental techniques and process modelling of sub-hourly and sub-kilometre land–atmosphere interactions, Biogeosciences, 17, 4375–4404, https://doi.org/10.5194/bg-17-4375-2020, 2020.

Vilà-Guerau de Arellano, J., van Heerwaarden, C. C., van Stratum, B. J. H., and van den Dries, K.: Atmospheric Boundary Layer: Integrating Air Chemistry and Land Interactions, Cambridge University Press, https://doi.org/10.1017/CBO9781316117422, 2015.

Vilà-Guerau de Arellano, J., Hartogensis, O., Benedict, I., de Boer, H., Bosman, P. J. M., Botía, S., Cecchini, M. A., Faassen, K. A. P., González-Armas, R., van Diepen, K., Heusinkveld, B. G., Janssens, M., Lobos-Roco, F., Luijkx, I. T., Machado, L. A. T., Mangan, M. R., Moene, A. F., Mol, W. B., van der Molen, M., Moonen, R., Ouwersloot, H. G., Park, S.-W., Pedruzo-Bagazgoitia, X., Röckmann, T., Adnew, G. A., Ronda, R., Sikma, M., Schulte, R., van Stratum, B. J. H., Veerman, M. A., van Zanten, M. C., and van Heerwaarden, C. C.: Advancing understanding of land–atmosphere interactions by breaking discipline and scale barriers, Annals of the New York Academy of Sciences, 00, 1–24, https://doi.org/https://doi.org/10.1111/nyas.14956, 2023.

Visser, A. J., Ganzeveld, L. N., Goded, I., Krol, M. C., Mammarella, I., Manca, G., and Boersma, K. F.: Ozone deposition impact assessments for forest canopies require accurate ozone flux partitioning on diurnal timescales, Atmospheric Chemistry and Physics, 21, 18393–18411, https://doi.org/10.5194/acp-21-18393-2021, 2021.

von Bobrutzki, K., Braban, C. F., Famulari, D., Jones, S. K., Blackall, T., Smith, T. E. L., Blom, M., Coe, H., Gallagher, M., Ghalaieny, M., McGillen, M. R., Percival, C. J., Whitehead, J. D., Ellis, R., Murphy, J., Mohacsi, A., Pogany, A., Junninen, H., Rantanen, S., Sutton, M. A., and Nemitz, E.: Field inter-comparison of eleven atmospheric ammonia measurement techniques, Atmospheric Measurement Techniques, 3, 91–112, https://doi.org/10.5194/amt-3-91-2010, 2010.

Webb, E., Pearman, G., and Leuning, R.: Correction of flux measurements for density effects due to heat and water vapour transfer., Quarterly Journal of the Royal Meteorological Society, 106, 85–100, 1980.

Wentworth, G., Murphy, J., Benedict, K., Bangs, E., and Collett Jr., J.: The role of dew as a night-time reservoir and morning source for atmospheric ammonia, Atmospheric Chemistry and Physics, 16, 7435–7449, https://doi.org/10.5194/acp-16-7435-2016, 2016.

Whitehead, J. D., Twigg, M., Famulari, D., Nemitz, E., Sutton, M. A., Gallagher, M. W., and Fowler, D.: Evaluation of Laser Absorption Spectroscopic Techniques for Eddy Covariance Flux Measurements of Ammonia, Environmental Science and Technology, 42, 2041–2046, https://doi.org/10.1021/es071596u, 2008.

Wichink Kruit, R. J. and van Pul, W. A. J.: Ontwikkelingen in de stikstofdepositie, Briefrapport 2018-0117, National Institute for Public Health and the Environment (RIVM), https://doi.org/10.21945/RIVM-2018-0117, 2018.

Wichink Kruit, R. J., van Pul, W. A. J., Otjes, R. P., Hofschreuder, P., Jacobs, A. F. G., and Holtslag, A. A. M.: Ammonia fluxes and derived canopy compensation points over non-fertilized agricultural grassland in The Netherlands using the new GRadient Ammonia - High Accuracy - Monitoring (GRAHAM), Atmospheric Environment, 41, 1275 – 1287, https://doi.org/https://doi.org/10.1016/j.atmosenv.2006.09.039, 2007.

Wichink Kruit, R. J., van Pul, W. A. J., Sauter, F. J., van den Broek, M., E., N., Sutton, M. A., Krol, M., and Holtslag, A. A. M.: Modeling the surface–atmosphere exchange of ammonia, Atmospheric Environment, 44, 945 – 957, https://doi.org/10.1016/j.atmosenv.2009.11.049, 2010.

Wilczak, J., Oncley, S., and Stage, S.: Sonic anemometer tilt correction algorithms., Boundary-Layer Meteorology, 99, 127–150, 2001.

Wyers, G., Otjes, R., and Slanina, J.: A continuous-flow denuder for the measurement of ambient concentrations and surface-exchange fluxes of ammonia, Atmospheric Environment. Part A. General Topics, 27, 2085–2090, https://doi.org/10.1016/0960-1686(93)90280-C, 1993.

Zhang, Q., Manzoni, S., Katul, G., Porporato, A., and Yang, D.: The hysteretic evapotranspiration — Vapor pressure deficit relation, Journal of Geophysical Research: Biogeosciences, 119, 125–140, https://doi.org/https://doi.org/10.1002/2013JG002484, 2014.

Zöll, U., Lucas-Moffat, A., Wintjen, P., Schrader, F., Beudert, B., and Bruemmer, C.: Is the biosphere-atmosphere exchange of total reactive nitrogen above forest driven by the same factors as carbon dioxide? An analysis using artificial neural networks, Atmospheric Environment, 206, 108–118, https://doi.org/10.1016/j.atmosenv.2019.02.042, 2019.